This manuscript is a non–peer-reviewed preprint submitted to EarthArXiv. It was submitted to Earth Surface Processes and Landforms (ESPL) for peer review.

Increasing temperatures controlled rockfall activity in the Rwenzori Mountains (Uganda) over the past 11,000 years

Audrey Margirier [1*], Konstanze Stübner [2], Christoph Schmidt [1], Johannes Lachner [2], Georg Rugel [2], Salome Oehler [1], Pontien Niyonzima [1], Rosemary Nalwanga [3], Anne Voigtländer [4]

[1] *Institute of Earth Surface Dynamics, University of Lausanne, Lausanne, Switzerland*
[2] *Institute of Ion Beam Physics and Materials Research, Helmholtz-Zentrum Dresden-Rossendorf, Dresden, Germany*
[3] *Department of Zoology, Entomology and Fisheries Sciences, Makerere University, Kampala, Uganda*
[4] *Earth and Environmental Sciences Area, Lawrence Berkeley National Laboratory, Berkeley, CA, USA*

Contact details:
Audrey Margirier: audrey.margirier@gmail.com (corresponding author)
Konstanze Stübner: k.stuebner@hzdr.de
Christoph Schmidt: christoph.schmidt@unil.ch
Johannes Lachner: j.lachner@hzdr.de
Georg Rugel: g.rugel@hzdr.de
Salome Oehler: salome.oehler@unil.ch
Pontien Niyonzima: pontien.niyonzima@unil.ch
Rosemary Nalwanga: roseastrid2013@gmail.com
Anne Voigtländer: avoigtlaender@lbl.gov

[*] Now at *Université Grenoble Alpes, Université Savoie Mont Blanc, CNRS, IRD, IFSTTAR. ISTerre, Grenoble, France*

Abstract

Rockfalls and other gravitational mass movements are expected to become more frequent under ongoing global warming in temperate and cold mountainous regions. In contrast, although high numbers of rockfalls are observed in humid tropical mountains, the processes controlling their occurrence remain poorly understood. These warmer regions offer valuable natural laboratories for anticipating the impacts of future warming on slope stability in currently colder environments. We used ^{10}Be surface exposure dating to establish a chronology for seven individual rockfall deposits in the Rwenzori Mountains (Uganda) and assess climatic controls on slope destabilisation. The combination of steep valley flanks and pervasive fracturing in the basement rocks makes the Rwenzori Mountains prone to rockfalls. The ^{10}Be ages range from 13.6 ± 0.9 ka to 1.0 ± 0.1 ka and cluster into three distinct periods: 11–9 ka, 7–5 ka and ~2 ka. These periods align with local temperature fluctuations, suggesting that rockfalls occurred episodically in response to Holocene temperature fluctuations. Early Holocene rockfall activity (~11–9 ka) likely reflects enhanced mechanical weathering and fracture propagation due to glacier retreat and freeze–thaw cycles. In contrast, mid-Holocene (7–5 ka) and late Holocene (~2 ka) rockfall activity coincide with warmer conditions that enabled chemical and biological weathering and enhanced subcritical crack growth, promoting fracture progression and slope destabilization. These results highlight the role of climate – especially temperature – driven chemical and biological weathering in preparing rock slope failures and rockfalls in tropical mountainous landscapes. With continued warming, chemical weathering may increasingly control rockfall activity in temperate and cold climates.

Keywords: rockfall deposits, ^{10}Be surface exposure dating, postglacial landscape, paleoclimate, progressive rock failure, chemical weathering, biological weathering, Rwenzori mountains

1. Introduction

In recent years, a high number of gravitational mass movements, such as landslides, debris flows, and rockfalls, triggered by rainfall events (e.g., Larsen and Simon, 1993; Zogning et al., 2007; Chen et al., 2015; Abancó et al., 2021; Zhuang et al., 2022) or earthquakes (e.g., Garwood et al., 1979; Chang et al., 2007; Faris and Fawu, 2014; Marc et al., 2015), have been reported in tropical regions. Rockfalls, however, result from the long-term interaction of multiple factors and rarely occur solely in response to the most recent trigger (e.g., Draebing and Krautblatter, 2019). Anticipating rockfall activity therefore requires understanding both structural preconditioning and progressive conditioning. In temperate and cold mountain regions, shifts in precipitation regimes, glacial debuttressing, permafrost degradation, and freeze–thaw cycles following deglaciation are widely recognized as key climatic controls on slope destabilization (e.g., Iverson, 2000; Patton et al., 2019; Hartmeyer et al., 2020). In these regions, changing climatic conditions, particularly warming, are expected to increase the frequency of potentially hazardous processes such as landslides and rockfalls (e.g., Hartmeyer et al., 2020; Pei et al., 2023; Jacquemart et al., 2024; Stoffel et al., 2024. While these climatic controls are well researched in cold and temperate climates, a general model for warmer or tropical climates is not established.

To forecast how mountainous landscapes may respond to climatic changes, from glacial to temperate to tropical climate, long-term records of climate and slope instability are needed (e.g., Gariano and Guzzetti, 2016; Pánek, 2019).

Constraining the timing of gravitational mass movements is crucial for deciphering their climatic controls over various timescales (e.g., Lang et al., 1999; Pánek, 2015). While considerable data exists for alpine, arctic, and arid regions (e.g., Zerathe et al., 2014; Margirier et al., 2015; Gariano and Guzzetti, 2016; Hilger et al., 2018; Pánek, 2019), chronological data in tropical regions are notably scarce despite documented occurrences of gravitational mass movements (e.g., Sewell et al., 2006; Gariano and Guzzetti, 2016; Pánek, 2019).

In this study we aim to establish a chronology of rockfalls in a region that experienced strong climatic changes. The Rwenzori Mountains, a glacially influenced tropical high mountain region characterized by steep slopes, a wet climate, and active faulting, present conditions favourable for slope instabilities, making them an excellent natural laboratory for such a study (Fig. 1). The upper part of the range hosts multiple well-preserved massive rockfall deposits that postdate the glacial sculpting of the landscape (Fig. 2). At lower elevations, gravitational mass movement deposits were likely eroded by ongoing river incision, while the lower parts of the catchments are marked by recent debris flows and active landslides (Jacobs et al., 2016, 2017). These ongoing processes pose significant hazards to local populations. For example, a flash flood event in the Nyamwamba catchment in 2013, caused several fatalities and extensive damage to infrastructure (e.g., Jacobs et al., 2016). Despite clear evidence of multiple past slope instabilities in the Rwenzori Mountains, chronological constraints exist for only a single landslide deposit only (Jackson et al., 2020). Several lakes in the region provide climatic archives, documenting local temperature and precipitation changes over the past 20,000 years (e.g., Garelick et al., 2022; Mason et al., 2024, refer to Fig. 1 for the location of these lakes within the Rwenzori Mountains). We hypothesized that linking these climatic records to the timing of rockfall events would provide first insights into the role of climatic variations in preconditioning rock slopes for failure.

We identified seven major rockfall deposits in the Rwenzori Mountains and used terrestrial cosmogenic nuclide (TCN) dating to constrain their chronology. Our results point to rising temperatures as a key preconditioning factor in tropical mountain environments.

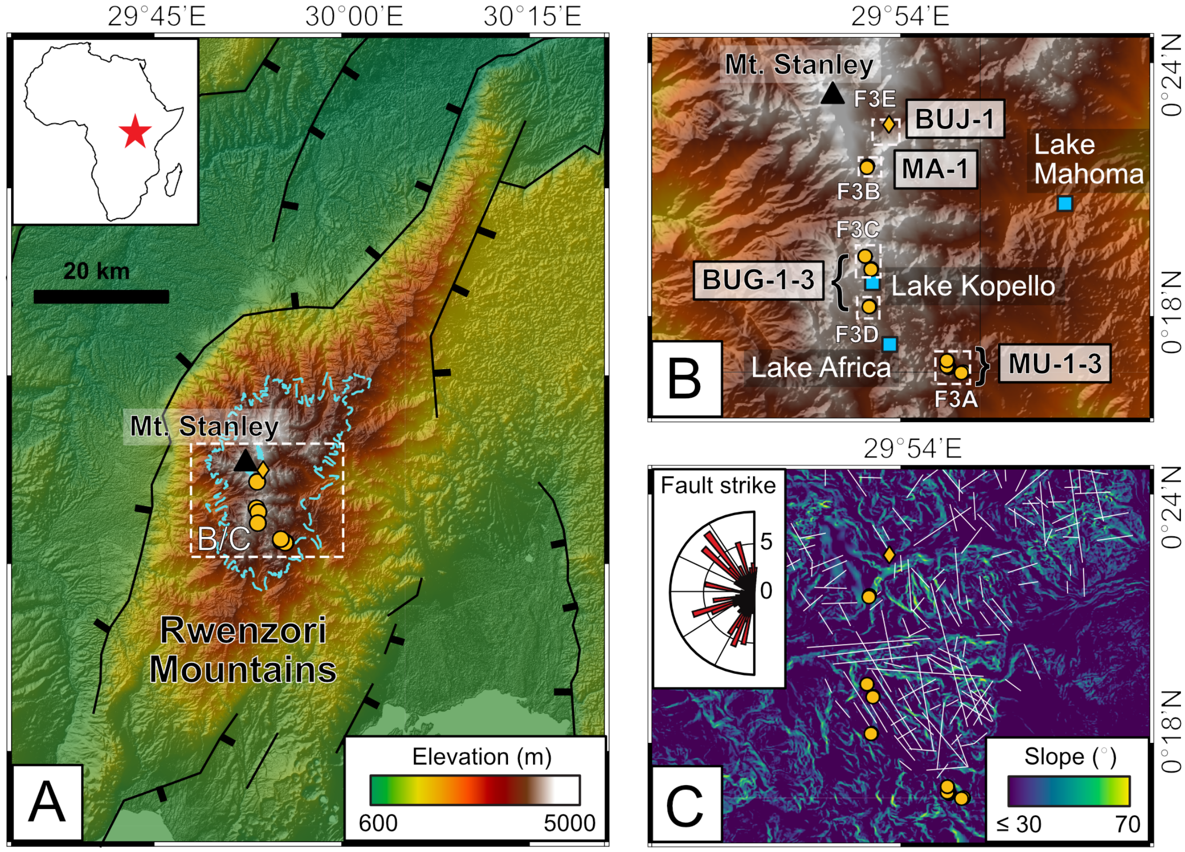

FIGURE 1. (A) Topographic map of the Rwenzori Mountains showing the location of the dated rockfall deposits (orange dots, this study) and a landslide deposit (orange square, BUJ-1; Jackson et al., 2020). The inset map shows the location of the study area within Africa. The topography is derived from the SRTM 1 Arc-Second Global DEM (30 m resolution; U.S. Geological Survey, 2000). The extent of Last Glacial maximum (LGM) glaciation is outlined in light blue, and present-day glacial remnants are shown as small light blue areas (RGI 7.0 Consortium, 2023). Active faults related to rifting are shown in black (Koehn et al., 2016). (B) Zoomed-in view of the high central Rwenzori region highlighting the location of the dated deposits and the lakes (blue diamonds) used for paleoclimatic reconstructions. (C) Same area as (B) showing dated

deposit locations, slope angles, and tectonic lineaments from Koehn et al. (2016), along with an inset rose diagram of fracture orientations from the same source.

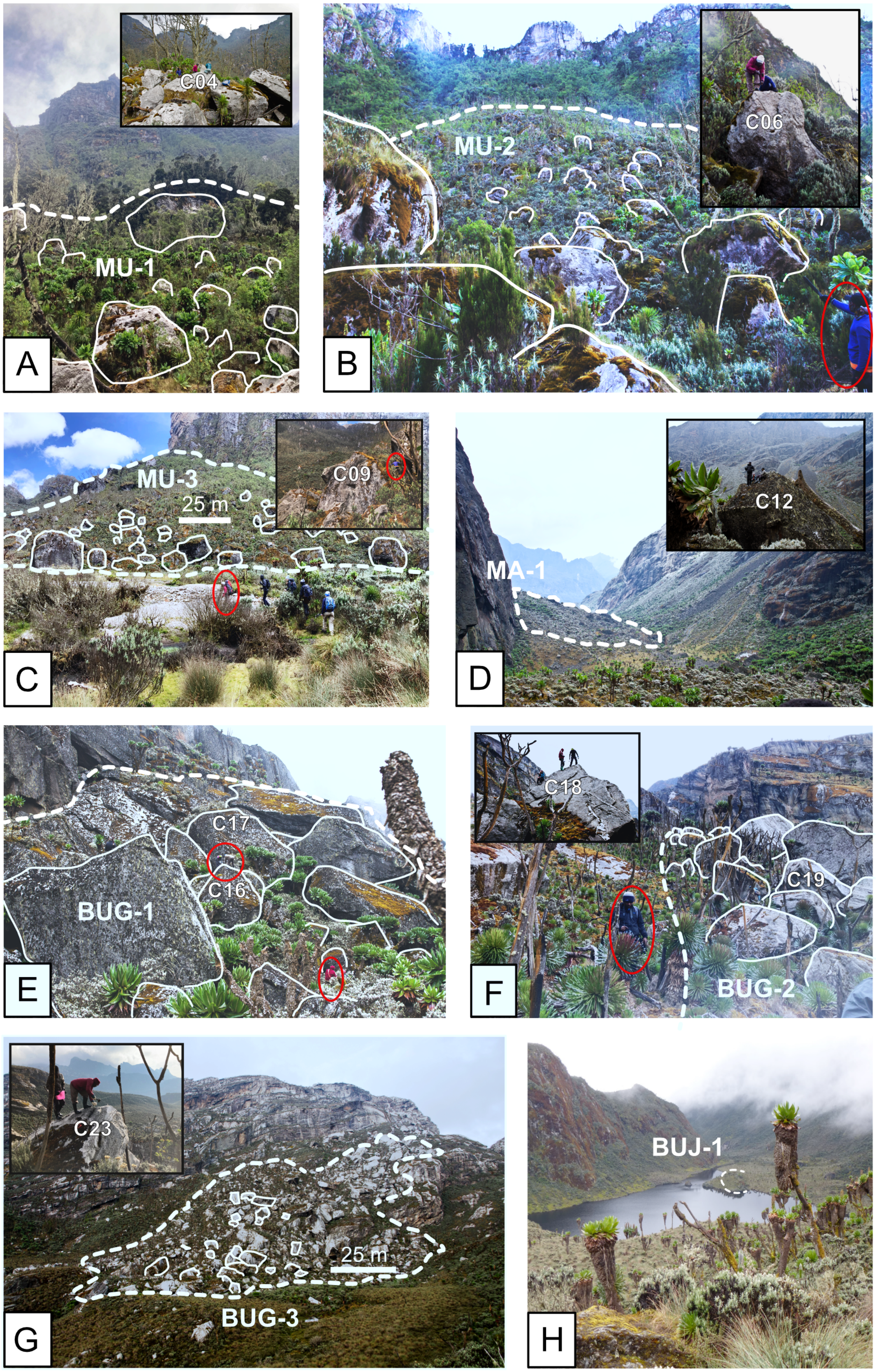
A
C04
MU-1
B
MU-2
C06
C
MU-3
25 m
C09
D
MA-1
C12
E
BUG-1
C17
C16
F
C18
C19
BUG-2
G
C23
25 m
BUG-3
H
BUJ-1

FIGURE 2. Photographs of the rockfall deposits. (A-C) Mutinda Valley: MU-1, MU-2, and MU-3 deposits. (D) Margherita Valley: MA-1 deposit. (E-G) Bugata Valley: BUG-1, BUG-2 and BUG-3 deposits. (H) Bujuku Valley: BUJ-1 deposit (photograph by Ingvar Backéus). Dashed white lines outline the extent of each deposit. Selected boulders are highlighted with white contours, and dated boulders are identified where possible (note that the prefix RWZ23- does not appear on the photographs). Insets show close-ups of boulder sampling. Individuals are circled in red to provide scale for both the deposits and the boulders.

2. Context

2.1 Geology and geomorphology

The Rwenzori Mountains, with elevations exceeding 5,000 m, are among the highest on the African continent, featuring more than 3,000 m of relief. Geologically, the Rwenzori represent an uplifted horst block within the western branch of the East African Rift system (Ring, 2008; Jess et al., 2020). The range is composed primarily of Archaean gneisses, Proterozoic schists, and Paleoproterozoic amphibolites (Koehn et al., 2016). The long-lived tectonic activity in the region has produced a dense network of fault lineaments cutting the crystalline basement. The upper part of the range is characterized by two dominant fault populations with steep planes oriented NNW–SSE and NNE–SSW, which accommodated normal and strike-slip motion. Additionally, a set of gently southward-dipping, E–W striking faults is present (Koehn et al., 2010, 2016). Despite the region's tectonic activity, only small-magnitude and deep earthquakes have been recorded near the Rwenzori Mountains (e.g., Maasha, 1975; Albaric et al., 2009; Lindenfeld et al., 2012).

The Rwenzori Mountains have been shaped by several glacial advances (e.g., Bauer et al., 2012). Large moraines are preserved in the eastern part of the mountains and controlled the formation of extensive swamps and bogs (e.g., Bauer et al., 2012; Jackson et al., 2020). U-shaped valleys are ubiquitous, highlighting the strong influence of past glaciations on the landscape (Bauer et al., 2012). These high-elevation (3500-4500 m asl) valleys preserve numerous rockfall deposits, providing evidence of past slope instability (i.e., Jackson et al., 2020). Based on ^{10}Be dating of boulders, an age of 11.0 ± 0.2 ka was determined for a rockfall deposit from the Bujuku Valley (Fig. 1; Jackson et al., 2020). At lower elevations (below ~3000 m asl) the relief is characterized by steep slopes and deep valleys incised by active river systems (e.g., Bauer et al., 2012). Below ~3500 m asl, climatic conditions favour dense mountain cloud forest vegetation, limiting the extent of bare rock exposure (e.g., Bauer et al., 2012; Roller et al., 2012). The overall denudation rates in the mountain range are low, with in situ-derived cosmogenic denudation rates ranging from 28 to 131 mm/kyr across the catchments (Roller et al., 2012).

The combination of inherited steep topography, active fluvial incision, high rainfall and seismic activity favours the occurrence of hazardous landslides, rockfalls, and frequent debris flows (e.g., Jacobs et al., 2016; Jacobs et al., 2017).

2.2 Climate and glaciations

The African continent has experienced dramatic climatic fluctuations over the past 20 kyr. During the African Humid period (~14.8 to 5.5 ka) the northward migration of the Intertropical Convergence Zone led to enhanced moisture availability and the expansion of lakes and wetlands in northern and equatorial Africa (De Menocal et al., 2000; Shanahan et al., 2015; De Menocal, 2015; Tierney et al., 2017). The timing and rates of the termination of the African Humid period varied spatially (e.g., Shanahan et al., 2015; Claussen et al., 2017). Available local climatic records from lake sediments provide high-resolution reconstructions of past temperature and hydrological changes in the Rwenzori Mountains (Garelick et al., 2022; Mason et al., 2024). Temperature reconstructions from Lake Mahoma (refer to Fig. 1 for location), based on the relative abundance of branched glycerol dialkyl glycerol tetraethers (brGDGT), show warming during the last global deglaciation (~21 – 7 ka), a temperature maximum in the mid-Holocene (~7 – 5 ka), and a cooling trend until the present (~5 – 0.2 ka; Garelick et al., 2022). The temperature reconstruction from Lake Mahoma aligns with the pollen record from the same site (Livingstone, 1967). Precipitation records from Holocene leaf wax hydrogen isotopic composition (δ^2H_{precip}) in Lake Mahoma, Lake Kopello, and Lake Africa (refer to Fig. 1 for locations) reveal intensified precipitation in the early Holocene (~11.7 – 8.2 ka), which gradually diminished through the middle to late Holocene (~8.2 ka – present) (Garelick et al., 2022; Mason et al., 2024). Today, the Rwenzori Mountains receive over 2500 mm of precipitation annually at high elevations (Osmaston, 1989; Russell et al., 2009). Precipitation in the Rwenzori Mountains is predominantly influenced by easterly monsoons, resulting in higher annual precipitation on the eastern slopes compared to the western side. Mean annual temperature at 4200 m asl is approximately 2 °C, with a lapse rate of ~0.67 °C per 100 m elevation (Osmaston 1965).

Moraine ^{10}Be exposure ages allow reconstructing the deglaciation history in the Rwenzori Mountains since the Last Glacial Maximum (LGM), locally known as Lake Mahoma Stage (e.g., Livingstone, 1967; Kelly et al., 2014; Jackson et al., 2020). During the LGM, all major valleys were glaciated, with glacier termini reaching elevations as low as ~2200 m asl in some valleys. The glacial retreat began at ~20 ka (Kelly et al., 2014; Jackson et al., 2019) and accelerated at ~18.5-18 ka (Jackson et al., 2020). By ~15–14 ka, glacier termini had retreated by more than 50% from their LGM extents. After a brief period of stability around ~15 ka, glacial retreat continued at slower rates. Glaciers then experienced rapid retreat after ~11.7 ka (Jackson et al., 2020). Before the 1950s, all six Rwenzori peaks were still glaciated, with ice tongues descending from Mounts Stanley, Speke, and Baker to elevations as low as 4,200 m asl (Kaser and Osmaston 2002). Currently, only small glaciers persist at high elevations in the Rwenzori Mountains (Fig. 1A; RGI 7.0 Consortium, 2023). The comparison of glacial extents with regional climate proxies suggests that the deglaciation dynamics are predominantly controlled by temperature changes, with precipitation playing a secondary role on glacial fluctuations (Jackson et al., 2020; Garelick et al., 2022). Temperature reconstructions indicate that the freezing-level height rose above the summit elevations of the Rwenzori Mountains between ~7 and 5 ka, likely causing complete deglaciation during this period (Garelick et al., 2022). Garelick et al. (2022) identify this mid-Holocene warming as an analogue for the glacial and environmental changes the Rwenzori Mountains are expected to experience in the coming decades.

2.3 Rockfall locations, deposit morphology and sources

Rockfalls have their source areas on steep mountain walls and cliffs, with deposit accumulating at the base of the slope. Their volume is largely controlled by geological factors such as lithology, fracture and joint spacing. On steep slopes, failure typically occurs through extensional fracturing, driven by the propagation of existing joints and fractures.

Based on field observations, all dated rockfall deposits (this study; Jackson et al., 2020) originate from steep (frequently exceeding 70°) to near-vertical cliff zones in the glacially shaped high elevation valleys of the Rwenzori Mountains. These steep slopes are not resolved by the 30m SRTM digital elevation models available for the region (SRTM 1 Arc-Second Global DEM; 30 m resolution; U.S. Geological Survey, 2000), as slope metrics are highly sensitive to the

DEM resolution (e.g., Voigtländer et al. 2024a). Consequently, in our morphometric analysis of rockfall source and deposition areas, slope was used as a spatial filter while all the subsequent analyses rely on elevation values. The mean, minimum, and maximum elevations of source cliffs were determined by applying a 35° slope threshold to the delimited upstream area of each deposit (Fig. 3).

Six rockfall deposits (MU-2, MU-3, MA-1, BUG-1, BUG-2, BUG-3; dated in this study) originated from cliffs aligned with the NNW–SSE structural trend either from northeast or southwest facing slopes, and two deposits (MU-1, BUJ-1; dated in this study and by Jackson et al., 2020 respectively) are sourced from north-facing slopes. The source areas of these rockfalls range from 3590 to 4619 m asl based on DEM analysis, (Fig. 3; Table S1).

In the Mutinda Valley, rockfall deposits MU-1 (Fig. 2A), MU-2 (Fig. 2B), and MU-3 (Fig. 2C) are located at elevations of ~3650–3700 m, ~3590–3650 m, and ~3650–3750 m asl, respectively. MU-1 likely originated from a steep north-facing slope between 3729 and 3930 m asl, MU-2 from a south-facing slope between 3621 and 3740 m asl, and MU-3 from a southwest-facing slope between 3681 and 3936 m asl (Table S1). These three deposits are vegetated and moss partially covers the boulder surfaces. The MU-1 deposit is characterized by a ridge along its southeastern margin and a relatively flat lobe, composed of boulders ranging from approximately 2 to 5 m in diameter (Fig. 2A). MU-2 forms a large, cone-shaped rockfall deposit of boulders measuring roughly 1 to 3 m in diameter (Fig. 2B). In contrast, MU-3 is composed of notably larger blocks, with several boulders exceeding 15 m in diameter (Fig. 2C).

In the Margherita Valley, we identified and sampled one major rockfall deposit, MA-1 at ~4100-4200 m asl which consists of boulders mostly ranging from ~1 to 5 m in diameter (Fig. 2D). It originated from a west-facing slope between 4188 and 4619 m asl (Fig. 3B). The deposit is vegetated. Moss and lichens partially cover the boulder surfaces.

We sampled three rockfalls in the Bugata Valley south of Weismann Peak. Deposit BUG-1 at ~4350-4400 m asl, closest (~500m) to the peak has a source area on southwest-facing slope between 4333 and 4459 m asl (Fig. 3C). Boulders range from ~3 to 15 m in diameter (Fig. 2E). Vegetation is sparse within the rockfall deposit, the boulders are partially covered with moss and lichens. At ~4150-4250 m asl and about 500m downstream, BUG-2 rockfall is deposited, and similarly sourced from a southwest-facing slope between 4206 and 4324 m asl (Fig. 3C). Boulders range from ~2 to 6 m in diameter (Fig. 2F). The deposit is more vegetated than BUG-1. The third rockfall deposit (BUG-3; ~4100-4200 m asl) lies 1.5 km south of BUG-2. It originated from an east-facing slope between 4205 and 4294 m asl (Fig. 3D). Boulders range from ~2 m to 10 m in diameter (Fig. 2G). The deposit is fully vegetated.

Situated ~2 km northeast of MA-1 rockfall deposit, BUJ-1 deposit (Fig. 2H) is located in the Bujuku Valley at ~3910-3920 m asl, it was previously described by Jackson et al. (2020) as a rockfall. The deposit partially dammed the valley and controlled the formation of Lake Bujuku. Based on aerial photograph analysis, Livingstone et al. (1967) proposed the BUJ-1 rockfall originated from the slopes of Mt. Baker. The north-facing source area would have been between ~3974 and 4651 m asl (Fig. 3E).

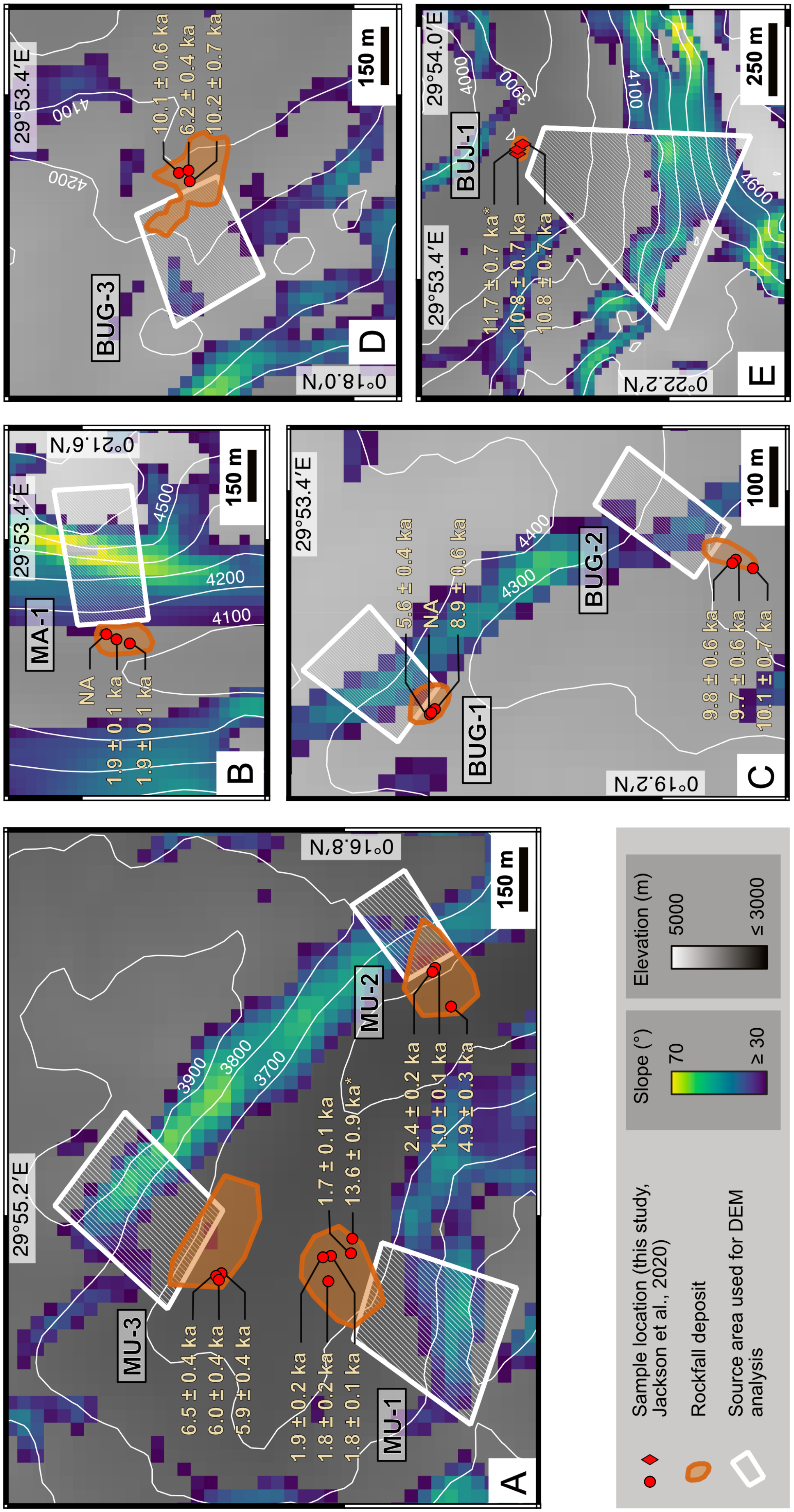
A
29°55.2′E
0°16.8′N
150 m
MU-3
6.5 ± 0.4 ka
6.0 ± 0.4 ka
5.9 ± 0.4 ka
MU-1
1.9 ± 0.2 ka
1.8 ± 0.2 ka
1.8 ± 0.1 ka
1.7 ± 0.1 ka
13.6 ± 0.9 ka*
MU-2
2.4 ± 0.2 ka
1.0 ± 0.1 ka
4.9 ± 0.3 ka
3900
3800
3700
B
29°53.4′E
0°21.6′N
150 m
MA-1
NA
1.9 ± 0.1 ka
1.9 ± 0.1 ka
4100
4200
4500
C
29°53.4′E
0°19.2′N
100 m
BUG-1
5.6 ± 0.4 ka
NA
8.9 ± 0.6 ka
BUG-2
9.8 ± 0.6 ka
9.7 ± 0.6 ka
10.1 ± 0.7 ka
4300
4400
D
29°53.4′E
0°18.0′N
150 m
BUG-3
10.1 ± 0.6 ka
6.2 ± 0.4 ka
10.2 ± 0.7 ka
4100
4200
E
29°53.4′E
29°54.0′E
0°22.2′N
250 m
BUJ-1
11.7 ± 0.7 ka*
10.8 ± 0.7 ka
10.8 ± 0.7 ka
4000
3900
4100
4600
Sample location (this study, Jackson et al., 2020)
Rockfall deposit
Source area used for DEM analysis
Slope (°)
70
≥ 30
Elevation (m)
5000
≤ 3000

FIGURE 3. Maps showing the approximate extent of the rockfall deposits and their potential source areas. Slope angles exceeding 35° are represented using a colour gradient. Contour lines (white) are calculated from the DEM. Individual boulder exposure ages are indicated on each panel. (A) Mutinda Valley: MU-1, MU-2, and MU-3 deposits. (B) Margherita Valley: MA-1 deposit. (C) Bugata Valley: BUG-1 and BUG-2 deposits. (D) Bugata Valley: BUG-3 deposit. (E) Bujuku Valley: BUJ-1 deposit (Jackson et al., 2020).

3. Methodology

Terrestrial cosmogenic nuclide (TCN) surface exposure dating is based on the accumulation of cosmogenic isotopes (such as in-situ produced ^{10}Be) in minerals exposed to cosmic rays at or near Earth’s surface (e.g., Gosse and Phillips, 2001; Bierman et al., 2002). This technique allows determining the time elapsed since a rock surface was first exposed, making it particularly effective for dating deposits resulting from gravitational mass movements such as rockfalls and landslides. In such contexts, measuring concentrations of in-situ produced ^{10}Be in quartz from rock surfaces enables the reconstruction of depositional ages following detachment and transport. This method assumes that the sampled surface was not previously exposed; to mitigate the potential influence of inherited nuclides (e.g., Hilger et al., 2019), multiple boulders from the same deposit are typically analysed (e.g., Zerathe et al., 2022). Cosmogenic dating has been successfully applied in diverse geomorphic settings to constrain the timing of slope failures (e.g., Cossart et al., 2008; Ivy-Ochs et al., 2009; Margirier et al., 2015; Zerathe et al., 2022).

3.1 Sampling strategy

A total of 3–5 samples were collected from each of seven distinct rockfall deposits from the eastern flank of the Rwenzori Mountains for TCN dating. We selected large boulders (>2 m) that showed minimal vegetation coverage (limited to moss and some lichens) and no indication of post depositional movement or alteration. No evidence of surface exfoliation or flaking of thin rock layers was observed in the field. All boulders within the rockfall deposits consist of gneiss, except for the Margherita Valley deposit (MA-1), which consists of amphibolite. We sampled the uppermost part (< 3 cm) of each selected boulder using a hammer and chisel. For the MA-1 deposit, two samples were specifically collected from quartz veins at the top of the boulders to ensure sufficient quartz content for the analysis. We recorded sample locations using a handheld GPS and measured the topographic shielding using a clinometer and compass. All boulders sampled from the rockfall deposits are located between 2622 and 4373 m asl.

3.2 ^{10}Be surface exposure dating

Sample preparation was conducted at the Institute of Earth Surface Dynamics (IDYST) at the University of Lausanne and at the Helmholtz-Zentrum Dresden-Rossendorf (HZDR). As most of the samples contained enough quartz, we extracted in situ produced beryllium-10 (^{10}Be) using the chemical procedures developed by Brown et al. (1991) and Merchel and Herpers (1999). The AMS ^{10}Be measurements were performed at the DREAMS facility of the Ion Beam Centre at the HZDR (Lachner et al., 2023) and data were normalized to the reference material SMD-Be-12 with a nominal ratio of $(1.704 \pm 0.030) \times 10^{-12}$ (Akhmadaliev et al., 2013). Analytical uncertainties include uncertainties associated with AMS counting statistics, AMS external error (1 %), standard reproducibility and chemical blank measurements ($^{10}Be/^{9}Be$ blank ranging from $3.14 \pm 1.29 \times 10^{-16}$ to $6.97 \pm 1.94 \times 10^{-16}$). External uncertainties include uncertainty in the production rate and uncertainty in the ^{10}Be decay constant. Exposure ages were calculated using the online calculator, version 3 (Balco et al., 2008) with the global production rates from Borchers et al. (2016) and the LSDn time-dependent scaling method (Lifton et al., 2014). In addition, we recalculated the ^{10}Be exposure ages reported by Jackson et al. (2020) using the same parameters to ensure consistency across datasets. The exposure ages were calculated under the assumption of zero surface erosion, which is justified given the young (postglacial) age of the deposits. At such timescales, and given the slow denudation rates (Roller et al., 2012), long-term average erosion would have a negligible impact on the ages.

4. Results

4.1 Rockfall ^{10}Be exposure ages

The ^{10}Be concentrations measured in all rockfall samples range from 1.93 ± 0.09 × 10^4 to 3.09 ± 0.07 × 10^5 atoms per gram of quartz (at g^{-1} qtz) (Table 1). Corresponding individual boulder ^{10}Be exposure ages range from 13.6 ± 0.9 to 1.0 ± 0.1 ka. When individual ^{10}Be exposure ages of boulders in a deposit are consistent within uncertainties, the mean age of the deposit is calculated as the average of the boulder ages. The reported uncertainty on the mean age of the deposit corresponds to the standard deviation of the individual boulder ages.

Rockfall deposits in the Mutinda Valley yield exposure ages ranging from 13.6 ± 0.9 to 1.0 ± 0.1 ka (Fig. 3A; Fig. 4; Table 1). The MU-1 deposit yields exposure ages ranging from 13.6 ± 0.9 to 1.7 ± 0.1 ka (Fig. 3A; Fig. 4; Table 1). Two samples from the ridge of MU-1 give exposure ages of 1.7 ± 0.1 ka and 13.6 ± 0.9 ka, while boulders from the lobe yield consistent exposure ages of 1.8 ± 0.1 ka, 1.8 ± 0.2 ka, and 1.9 ± 0.2 ka. Excluding the older exposure age from the ridge (13.6 ± 0.9 ka; RWZ23-C01), the ages are consistent within uncertainties, the mean age of the deposit is thus 1.8 ± 0.1 ka. The MU-2 deposit shows greater age dispersion. The lowest boulder (RWZ23-C08; 3593 m asl) gives an exposure age of 4.9 ± 0.3 ka, while the two higher boulders (RWZ23-C06 and RWZ23-C07; 3622–3625 m asl) yield younger exposure ages of 1.0 ± 0.1 ka and 2.4 ± 0.2 ka (Fig. 3A; Fig. 4). The MU-3 deposit yields consistent exposure ages of 5.9 ± 0.4 ka, 6.0 ± 0.4 ka and 6.5 ± 0.4 ka (Fig. 3A; Fig. 4), resulting in a mean age of 6.1 ± 0.3 ka.

In the Margherita Valley, the MA-1 deposit was dated using two boulders, both yielding ages of 1.9 ± 0.1 ka (Fig. 3B; Fig. 4). A third sample did not contain sufficient quartz for analysis.

Rockfall deposits in the Bugata Valley yield exposure ages ranging from 5.6 ± 0.4 to 10.2 ± 0.7 ka. The BUG-1 deposit was dated using two boulders, yielding exposure ages of 5.6 ± 0.4 ka and 8.9 ± 0.6 ka (Figs. 3C, 4). Quartz content in a third sample was too low for analysis. The BUG-2 deposit shows consistent exposure ages of 9.7 ± 0.6 ka, 9.8 ± 0.6 ka, and 10.1 ± 0.7 ka, with a mean age of 9.9 ± 0.2 ka (Figs. 3C, 4). For the BUG-3 deposit, three boulders yield exposure ages of 6.2 ± 0.4 ka, 10.1 ± 0.6 ka, and 10.2 ± 0.7 ka, with the latter two consistent within uncertainties (Fig. 3C; Fig. 4).

The ^{10}Be exposure ages of individual boulders from rockfall deposits in the Rwenzori mountains cluster into three distinct periods: ~11–9 ka, 7–5 ka, and ~2 ka (Fig. 4).

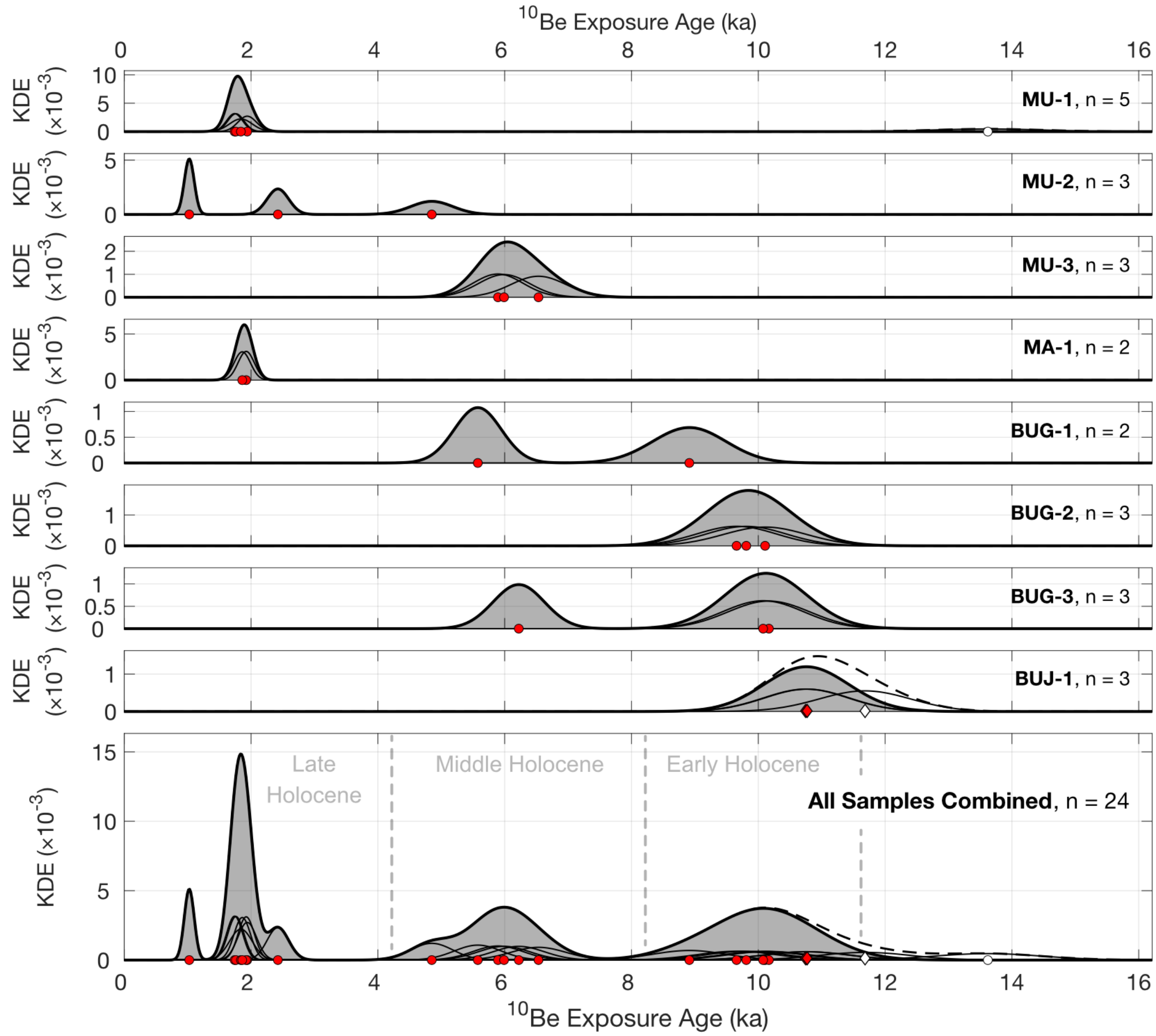

FIGURE 4. Surface exposure ages of rockfall deposits from the Rwenzori Mountains. Kernel probability-density estimation (KDE) plots of exposure ages for individual rockfall deposits: three from Mutinda Valley (MU-1, MU-2, MU-3), one from Margherita Valley (MA-1), three from Bugata Valley (BUG-1, BUG-2, BUG-3), one from Bujuku Valley (BUJ-1; Jackson et al., 2020). (I) Combined probability density plot for all deposits. Thin black lines correspond to individual exposure ages. Red circles and diamonds represent individual exposures ages of rockfalls from this study and from Jackson et al. (2020) respectively. White markers indicate exposure ages interpreted as outliers,

specifically RWZ23-C01 (MU-1) and RZ-16-35 (BUJ-1) dated at 13.6 ± 0.9 and 11.7 ± 0.7 ka respectively (see text for details). Thick black curves and filled area correspond to the summed probability density functions excluding these outliers, dashed black curves correspond to the summed probability density including all the ages.

4.2 Recalculated rockfall ages

Jackson et al. (2020) dated three boulders from a rockfall deposit (BUJ-1) in the Bujuku Valley. The recalculated ages for the three boulders are of 10.8 ± 0.7 ka, 10.8 ± 0.7 ka and 11.7 ± 0.7 ka, with the three ages consistent within uncertainties. Our re-calculated ages are slightly younger than the published ages (10.9 ± 0.7 ka, 10.9 ± 0.7 ka and 11.9 ± 0.7 ka), because we take into account magnetic field strength variation. Jackson et al. (2020) excluded the older age (recalculated at 11.7 ± 0.7 ka) based on the local ^{10}Be moraine chronology and evidence that the rockfall occurred after the glacier retreated from the Bujuku Valley. Following this reasoning, we excluded the older age and obtain a rockfall deposit age of 10.8 ± 0.1 ka. This age aligns with the older age cluster (~11–9 ka) defined by the seven rockfall deposits dated in this study (Fig. 3).

5. Discussion

5.1 Chronology of rockfall activity

Individual ^{10}Be exposure ages from boulders consistently cluster at ~11–9 ka, 7–5 ka, and ~2 ka (Fig. 4), suggesting discrete phases of enhanced rockfall activity. Within four deposits (MU-3, MA-1, BUG-2, BUJ-1), the exposure ages are consistent within their uncertainties, indicating that the boulders were likely destabilized and exposed during single, short-lived events. In contrast, the greater age dispersion observed in deposits MU-1, MU-2, BUG-1, and BUG-3 suggests that these exposure ages reflect multiple rockfall events, post depositional remobilisation of the boulders, or inheritance from pre-exposed surfaces. While most exposure ages from these deposits fall within the main age clusters, two outliers stand out: one at 13.6 ± 0.9 ka (MU-1) and another at 1.0 ± 0.1 ka (MU-2). The 13.6 ± 0.9 ka age from MU-1 is inconsistent with other ages from both the ridge and lobe of MU-1. Based on the morphology of the deposit and the consistency of the remaining ages, we attribute this age to inherited cosmogenic nuclides concentration acquired prior to deposition. We therefore exclude it from further chronological interpretation. MU-2 corresponds to a large cone-shape rockfall deposit where three dated boulders yield distinct ages (4.9 ± 0.3, 2.4 ± 0.2 and 1.0 ± 0.1 ka). The cone-shaped morphology of this deposit in conjunction with the boulder age distribution with the youngest age at the bottom and the oldest at the top suggests that this deposit does, in fact, not represent a discrete rockfall event but results from prolonged, intermittent rockfall activity. Post-depositional remobilization, however, cannot be fully excluded. The age dispersion in deposits BUG-1 and BUG-3 likely reflects multiple destabilization events. The older ages may record the combined history of two rockfall episodes: initial exposure on the scarp following an early event, and subsequent exposure on the deposit after a second event, which is recorded by the younger ages.

5.2 Comparison of the rockfall chronology with climate records

The first phase of rockfall activity (~11–9 ka) coincides with a period of increasing temperatures, as inferred from the local lake sediment record (Fig. 5; Garelick et al., 2022). Comparison of the ^{10}Be exposure ages of rockfall deposits with moraine chronologies that constrain the timing of deglaciation (Fig. 5) indicates that this initial phase of slope failure occurred shortly after a major glacial retreat at high elevations (~4000 m), as documented by Jackson et al. (2020). Subsequent rockfall activity phases, dated to 7–5 ka and ~2 ka, correspond to the mid-Holocene thermal maximum and a short-lived late Holocene warming anomaly, respectively, according to the paleotemperature reconstruction of Garelick et al. (2022). This suggests a strong temperature control of rockfall conditioning.

Although the Rwenzori Mountains experienced persistently high precipitation levels throughout the Holocene, hydroclimatic conditions have varied over time. Hydrogen isotope records from terrestrial leaf waxes preserved in sediment cores from three local lakes (locations in Fig. 1B) show a consistent temporal variation between dryer and wetter phases (Mason et al., 2024). Relatively dry conditions prevailed around 11 ka, followed by a transition to wetter conditions between 10 and 6 ka, and a return to drier conditions beginning around 5 ka (Fig. 5, different colours distinguish individual lake records; Mason et al., 2024). The earliest rockfall phase (~11-9 ka) coincides with a wetter phase relative to the late Holocene and a period of rising temperatures. The two later phases (7–5 ka and ~2 ka) occurred under increasingly drier conditions, but during generally warmer temperatures. Precipitation variability does not relate directly to the timing of rockfall events in the Rwenzori Mountains. This contrasts with observations from other mountain regions, such as the European Alps or the Andes, where slope instabilities, like rockfalls and landslides, are often associated with wetter climatic phases (e.g., Trauth et al., 2003; Zerathe et al., 2014; Margirier et al., 2015). The persistent humidity of the Rwenzori region may reduce the sensitivity of slope stability to precipitation variability, thereby enhancing the relative influence of temperature-related conditioning mechanisms.

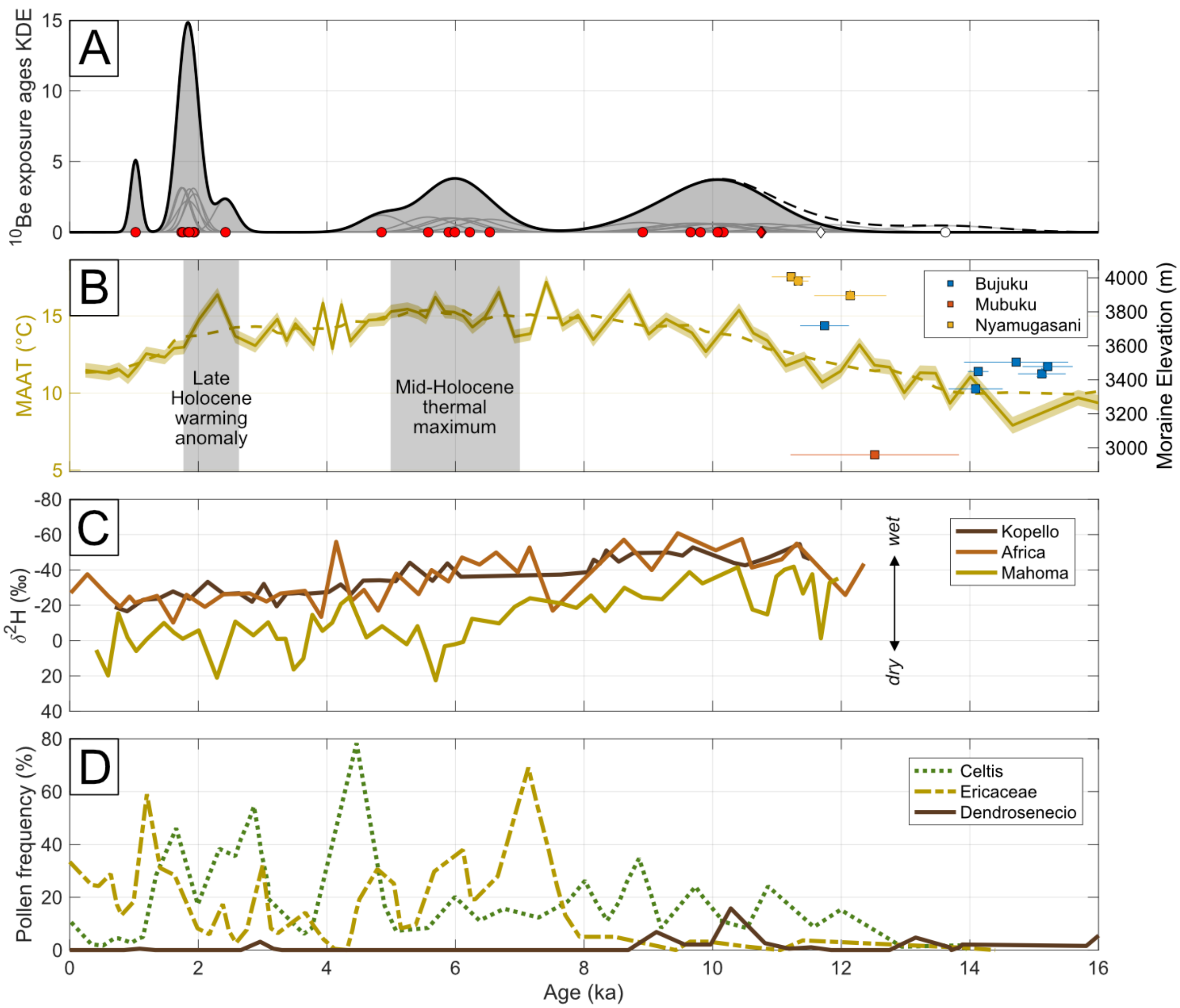

FIGURE 5. Surface exposure ages of rockfall deposits and Holocene climatic records from the Rwenzori Mountains. (A) Kernel probability-density estimation (KDE) plot of surface exposure ages. Red circles and diamonds represent individual ages from this study and Jackson et al. (2020) respectively; white markers denote ages interpreted as outliers. Thin black lines represent KDE for individual ages, while the thick black curve and shaded area represent the summed KDE excluding outliers. (B) Mean annual air temperature (MAAT) reconstructions from Lake Mahoma, derived from the relative abundance of branched glycerol dialkyl glycerol tetraethers (brGDGT)

(Garelick et al., 2022). Temperatures and associated uncertainties were recalculated using the Zhao et al. (2023) calibration by James Russell (pers. comm.). The solid line represents the temperature record, with the shaded yellow area indicating the corresponding 2-sigma uncertainty. The dashed line shows the running mean of the temperature data. Vertical grey bands highlight warm climatic phases (Garelick et al., 2022). The temperature reconstruction is shown in conjunction with moraine chronologies that constrain the timing of deglaciation (Jackson et al., 2020). Moraines from the Bujuku Valley are shown in blue, those from Mubuku in red, and those from Nyamugasani in yellow. (C) Hydrogen isotope records from terrestrial leaf waxes preserved in sediment cores from three local lakes: Kopello (4017 m asl, dark brown), Africa (3895 m asl, orange), and Mahoma (2990 m asl, yellow) (Mason et al., 2024). (D) Panel adapted from Garelick et al. (2022). Pollen reconstructions from Lake Mahoma (Livingstone, 1967). Pollen frequency measures how many grains of each pollen type are present in a given sediment volume. The three pollen types correspond to plants growing today at distinct Rwenzori elevations: high (Dendrosenecio), mid (Ericaceae), and low (Celtis).

5.3 Structural and tectonic controls on the rockfalls

Steep glacial valley flanks and geologic structures, like foliation, veins, and pervasive pre-existing fractures showcase structural controls on rockfall in the Rwenzori Mountains.

Six out of seven rockfall deposits, dated in this study as well as BUJ-1 originated from cliffs whose orientations align with the dominant fracture sets (Figs. 1C, 6A). Notably, valley orientations are generally parallel to these fracture sets (Koehn et al., 2010, 2016), suggesting a strong structural control on both landscape morphology and rockfall source areas. The pervasive pre-existing fracturing in the basement rocks provides pathways for weathering and fracture propagation, thereby promoting mechanical destabilization.

We find no relationship between deposit age and the aspect of the source areas (Fig. 6A). A weak correlation is observed between the elevation of rockfall source areas and the exposure ages of their deposits, with older ages (>8 ka) generally originating from higher elevations (between 3900 and 4620 m asl), whereas younger ages are predominantly associated with lower-elevation sources (below 3900 m asl) (Fig. 6B).

While topography and inherited tectonic structures control the spatial pattern of rockfall activity in the Rwenzori Mountains, they do not explain the conditioning of the slopes and timing of the observed activity.

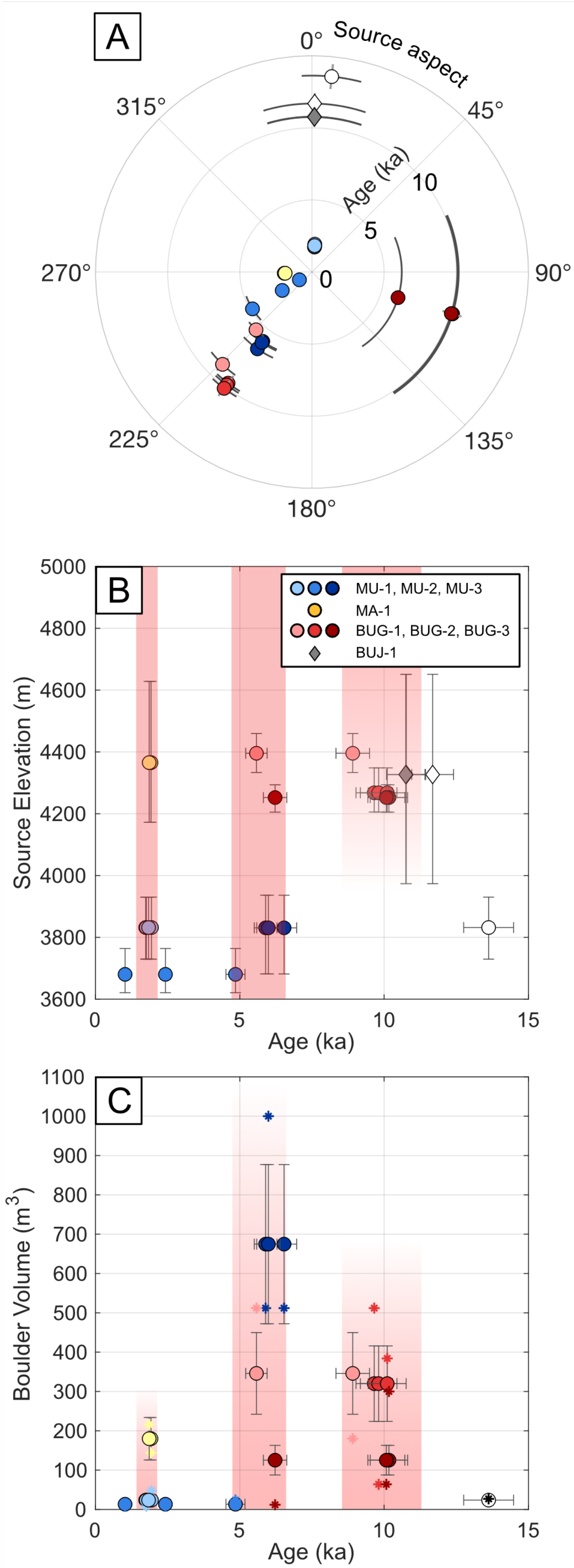
A
0°
Source aspect
315°
45°
Age (ka)
10
5
0
270°
90°
225°
135°
180°
B
MU-1, MU-2, MU-3
MA-1
BUG-1, BUG-2, BUG-3
BUJ-1
Source Elevation (m)
Age (ka)
C
Boulder Volume (m3)
Age (ka)

551

FIGURE 6. (A) Exposure ages plotted as a function of the slope aspect of the rockfall source areas (slope >35°). Angular and radial error bars represent aspect and age uncertainties, respectively. (B) Exposure ages of individual boulders plotted against the elevation of their source cliffs. Different colours and shapes distinguish individual rockfall deposits, and outliers are shown with white-filled symbols. Vertical error bars indicate the elevation range of each source area (slope >35°). Red shaded bands highlight the three age clusters identified in Figure 4. (C) Exposure ages of individual boulders plotted against the volume of the boulders. The uncertainty in volume is estimated as 30% of the measured value. Circles and diamonds represent the mean dated boulder volume for each rockfall deposit, while stars indicate individual dated boulder volume.

5.4 Climatic controls on rockfall preconditioning

Steeply dipping joints and faults in the Rwenzori Mountains (e.g., Koehn et al., 2010, 2016) predefined weaknesses in the rock slopes. Once fractures are persistent, rock bridges broken, and friction decreased, rockfalls can happen any time. The progressive rock degradation leading to this can be mechanically, chemically, and biologically enhanced. The mechanisms that promote the progression are sensitive to environmental conditions, including temperature, moisture, and biological activity, which varied throughout the Holocene (Fig. 5). In Figure 7, we present a first conceptual model of the temporal evolution of potential conditioning controls on rockfall activity in relation with temperature.

The first phase of rockfall activity (~11–9 ka) occurred during a prolonged period of rising temperatures (Fig. 5). It postdates shortly the local glacier retreat, as inferred from dated moraines at relevant elevations (Jackson et al., 2019, 2020). This early Holocene phase of rockfall activity was restricted to high elevations (Fig. 6B), and likely corresponds to the widely discussed postglacial, permafrost or paraglacial geomorphic slope adjustments (e.g., Ballantyne, 2002; Cossart et al., 2008; McColl, 2012; McColl and Davies, 2013; Dixon et al., 2024; Krautblatter et al., 2013). Permafrost conditions likely persisted in the high-elevation rockfall source areas following glacial retreat. Available meltwater or precipitation could have infiltrated existing fractures, enabling freeze–thaw processes to progressively destabilize the rock slope. Water-filled cracks expand and contract due to volumetric expansion during the phase transition from water to ice, which mechanically propagates fractures (Krautblatter et al., 2013). In addition, the presence of water reduces the rock strength and promotes localized failure (Voigtländer et al., 2018, 2020). These predominantly mechanical controls and physical weathering likely preconditioned early Holocene slope destabilisation (Fig. 7), similar to present-day conditions in the European Alps, Himalaya and Arctic (e.g., Regmi and Watanabe, 2009; Grämiger et al., 2017; Hilger et al., 2018; Hartmeyer et al., 2020).

The second phase of rockfall activity (7–5 ka) coincides with the mid-Holocene climatic optimum during which temperatures were ~3 °C higher than in the late Holocene (Fig. 5C; Garelick et al., 2022). Such elevated temperatures would have raised the freezing level above 5000 m (Garelick et al., 2022), making freeze–thaw processes an unlikely control in this and the subsequent rockfall phase (~2 ka). The second phase followed local deglaciation and an initial phase of rockfall activity that was mechanically preconditioned, e.g., by freeze–thaw processes. Glacial erosion and mechanical weathering provided fresh mineral surfaces with high chemical reactivity, making chemical enhancement of fracture growth a likely mechanism for progressive destabilization. The mid-Holocene warming was also accompanied by an upward shift in vegetation zones (Fig. 5; Livingstone, 1967), evidenced by an increase in Celtis pollen, characteristic of present-day low elevations, alongside a decline in Ericaceous pollen, typical of mid-elevation vegetation (Fig. 5D). This vegetation shift likely introduced biologically mediated processes contributing to slope destabilization. Elevated temperatures and enhanced biological activity in the Rwenzori Mountains during the mid Holocene likely promoted intensified chemical weathering. Progressive fracturing, or subcritical crack growth, has been shown to progress faster when chemically enhanced (e.g., Eppes & Keanini, 2017; Gerber & Scheidegger, 1969). Chemical and bio-chemical mechanisms include enhanced dissolution at the facture tips (stress corrosion), as well as wedging due to crystallization pressure and volumetric strain of precipitates in the fracture (Figure 7). In silicate rocks, elevated temperature increases chemical reaction kinetics, promoting the formation of secondary, soil-forming, minerals such as clays (e.g., White and Blum, 1995; Deng et al., 2022), which in turn promotes biological activity. Although rates of chemically enhanced crack growth in natural settings remain poorly constrained, laboratory and modeling studies have suggested propagation rates on the order of several millimeters per year, with a strong temperature dependence (e.g., Atkinson, 1984; Eppes & Keanini, 2017). Field based quantification of rates of chemically or biologically enhanced rock fracturing, and thus chemo-mechanical coupled processes remains a key challenge in current research.

The third phase of rockfall activity (~2 ka) occurred during slightly dryer climate, following a prolonged period of likely extended chemical weathering, including mineral leaching, dissolution and precipitation of secondary minerals which left the preexisting fractures likely near-equilibrium chemical conditions. We therefore propose a stronger control of biologically mediated chemo-mechanical mechanisms during the third phase of rockfall activity (Fig. 7). In this context, diffusion-controlled leaching of minerals may continue within preexisting fractures, increasing in porosity and reducing mechanical strength. In addition, dryer conditions favour the precipitation and crystallisation of secondary minerals in fractures (e.g., Walter et al., 2018; Hayes et al., 2019). This mineral precipitation can lead to volumetric expansion and fracture propagation. Over time, these processes weaken rock bridges, open secondary fractures, and promote wedging apart of blocks, ultimately contributing to rockfall susceptibility. The prolonged action of biologically mediated chemo-mechanical mechanisms on fractures likely explains the smaller boulder sizes observed in the third rockfall activity phase (Fig. 6C). Extended time for (bio)chemical reactions, probably allowed to form soil-like material in the fractures in which vegetation can grow. While soils are usually assumed to limit weathering (e.g., Hartmann et al., 2014), vegetation rooted in fractures can enhance local water retention, intensify chemical reactions, and exert mechanical strain, thus sustaining localized zones of rock weakening. Additional biologically mediated effects, such as those driven by microorganisms, may contribute to weathering and fracture propagation but their role remains a current research frontier (e.g., Wild et al., 2022; Voigtländer et al., 2024).

Overall, the preconditioning of slopes for destabilisation appears to be strongly influenced by Holocene climate, with temperature acting as the dominant factor.

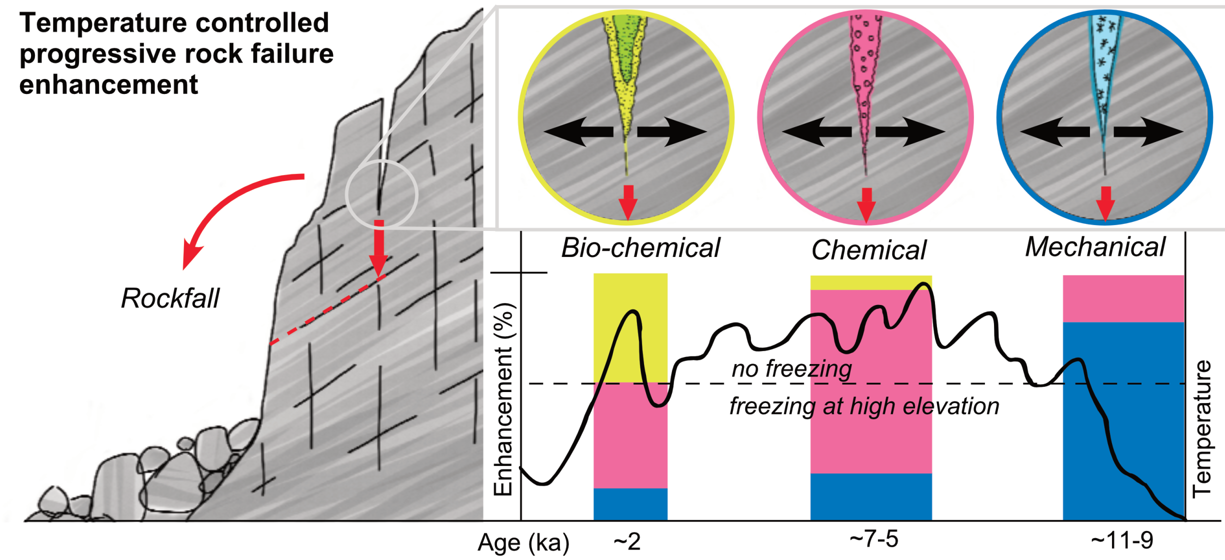

FIGURE 7. Conceptual sketch of temperature-controlled mechanisms enhancing progressive rock failure. Temperature and its temporal evolution enable mechanical, chemical or bio-chemical enhancement of fracture progression.

6. Conclusions

With current warming trends, temperatures in tropical high-mountain regions are projected to reach mid-Holocene levels within the coming decades. In the Rwenzori Mountains, contemporary warming has already led to glacier shrinkage and temperature conditions comparable to those of the early Holocene. This positions the Rwenzori as a valuable natural analogue for understanding how temperature-driven slope destabilization may evolve under ongoing and future climate change, both in tropical settings and in presently colder mountain environments.

The combination of steep valley flanks and pervasive pre-existing fracturing in the basement rocks makes the Rwenzori Mountains particularly prone to rockfalls. The ^{10}Be exposure ages of eight rockfall deposits cluster into three distinct periods: 11–9 ka, 7–5 ka, and ~2 ka. The alignment between these ages and regional temperature records suggests that major rockfall events occurred episodically in response to Holocene climatic fluctuations. We suggest that conditioning of slopes toward failure is strongly influenced by climate, especially temperature, that controls mechanical, chemical, and biological enhancement of progressive rock degradation.

These findings highlight the coupled influence of inherited tectonic structures and climate-driven processes in controlling slope instability in tropical mountain landscapes. Based on our results, we suggest that rising temperatures will likely enhance chemical and biological weathering, increasing the risk of future slope failures under ongoing climate change.

Acknowledgements

A. Margirier has received funding from the European Union's Horizon 2020350 research and innovation programme under the Marie Sklodowska-Curie grant agreement No 101066908. A.Voigtländer was supported by the US Department of Energy (DOE), the Office of Basic Energy Sciences, Chemical Sciences, Geosciences, and Biosciences Division under Contract Number DE-AC02-05CH11231 to Lawrence Berkeley National Laboratory.

This work was partially supported by the Swiss National Science Foundation (SNSF) under the grant number 200021_204236/1. Sampling was conducted with permission from Rwenzori Mountains National Park. We thank L. Rodari and K. Dyba for their valuable assistance with sample processing. Parts of this research were carried out at the Ion Beam Centre (IBC) at the Helmholtz-Zentrum Dresden-Rossendorf e. V., a member of the Helmholtz Association. We would like to thank the DREAMS operator team for their assistance with AMS-measurements.

Authors contributions

Audrey Margirier: conceptualization, data curation, formal analysis, investigation, project administration, visualization, writing – initial draft, writing – review & editing. **Konstanze Stübner:** investigation, writing – review & editing. **Christoph Schmidt:** investigation, project administration, writing – review & editing. **Johannes Lachner:** investigation, resources, writing – review & editing. **Georg Rugel:** investigation, resources. **Salome**

Oehler: investigation, writing – review & editing. **Pontien Niyonzima:** investigation. **Rosemary Nalwanga:** resources. **Anne Voigtländer:** investigation, visualization, writing – initial draft, writing – review & editing.

Data availability statement

The ^{10}Be data, morphometric analysis of rockfall source areas and shapefiles of source areas employed for the analysis are provided in the Supplementary Material and will be deposited in the Zenodo repository upon acceptance of the publication.

Funding statement

Funding was provided by the European Union's Horizon 2020350 research and innovation programme (Marie Sklodowska-Curie, grant agreement No. 101066908), the US Department of Energy (DOE), the Office of Basic Energy Sciences, Chemical Sciences, Geosciences, and Biosciences Division (contract No DE-AC02-05CH11231) and the Swiss National Science Foundation (grant No. 200021_204236/1).

Conflict of Interest Statement

This manuscript contains original data and interpretations, is not under consideration elsewhere, and does not overlap with any of our recent publications. The authors have no competing interests to declare.

References

Abancó C, Bennett GL, Matthews AJ, Matera MAM, Tan FJ. 2021. The role of geomorphology, rainfall and soil moisture in the occurrence of landslides triggered by 2018 Typhoon Mangkhut in the Philippines. Natural Hazards and Earth System Sciences 21 : 1531–1550. DOI: 10.5194/nhess-21-1531-2021

Akhmadaliev S, Heller R, Hanf D, Rugel G, Merchel S. 2013. The new 6MV AMS-facility DREAMS at Dresden. Nuclear Instruments and Methods in Physics Research Section B: Beam Interactions with Materials and Atoms **294** : 5–10. DOI: 10.1016/j.nimb.2012.01.053

Albaric J, Déverchère J, Petit C, Perrot J, Le Gall B. 2009. Crustal rheology and depth distribution of earthquakes: Insights from the central and southern East African Rift System. Tectonophysics 468 : 28–41. DOI: 10.1016/j.tecto.2008.05.021

Atkinson BK. 1984. Subcritical crack growth in geological materials. Journal of Geophysical Research: Solid Earth **89** : 4077–4114. DOI: 10.1029/JB089iB06p04077

Balco G, Stone JO, Lifton NA, Dunai TJ. 2008. A complete and easily accessible means of calculating surface exposure ages or erosion rates from 10Be and 26Al measurements. Quaternary Geochronology 3 : 174–195. DOI: 10.1016/j.quageo.2007.12.001

Ballantyne CK. n.d. Paraglacial geomorphology

Bauer FU, Karl M, Glasmacher UA, Nagudi B, Schumann A, Mroszewski L. 2012. The Rwenzori Mountains of western Uganda – Aspects on the evolution of their remarkable morphology within the Albertine Rift. Journal of African Earth Sciences 73–74 : 44–56. DOI: 10.1016/j.jafrearsci.2012.07.001

Bierman PR, Caffee MW, Davis PT, Marsella K, Pavich M, Colgan P, Mickelson D, Larsen J. 2002. Rates and Timing of Earth Surface Processes From In Situ-Produced Cosmogenic Be-10. Reviews in Mineralogy and Geochemistry 50 : 147–205. DOI: 10.2138/rmg.2002.50.4

Borchers B, Marrero S, Balco G, Caffee M, Goehring B, Lifton N, Nishiizumi K, Phillips F, Schaefer J, Stone J. 2016. Geological calibration of spallation production rates in the CRONUS-Earth project. Quaternary Geochronology 31 : 188–198. DOI: 10.1016/j.quageo.2015.01.009

Brown ET, Edmond JM, Raisbeck GM, Yiou F, Kurz MD, Brook’ EJ. n.d. Examination of surface exposure ages of Antarctic moraines using in situ produced “Be and 26A

Chang K-T, Chiang S-H, Hsu M-L. 2007. Modeling typhoon- and earthquake-induced landslides in a mountainous watershed using logistic regression. Geomorphology 89 : 335–347. DOI: 10.1016/j.geomorph.2006.12.011

Chen C-W, Saito H, Oguchi T. 2015. Rainfall intensity–duration conditions for mass movements in Taiwan. Progress in Earth and Planetary Science 2 : 14. DOI: 10.1186/s40645-015-0049-2

Claussen M, Dallmeyer A, Bader J. 2017. Theory and Modeling of the African Humid Period and the Green Sahara . Oxford University Press [online] Available from: http://oxfordre.com/climatescience/view/10.1093/acrefore/9780190228620.001.0001/acrefore-9780190228620-e-532 (Accessed 30 June 2025)

Cossart E, Braucher R, Fort M, Bourlès DL, Carcaillet J. 2008. Slope instability in relation to glacial debuttressing in alpine areas (Upper Durance catchment, southeastern France): Evidence from field data and 10Be cosmic ray exposure ages. Geomorphology 95 : 3–26. DOI: 10.1016/j.geomorph.2006.12.022

De Menocal PB. 2015. End of the African Humid Period. Nature Geoscience 8 : 86–87. DOI: 10.1038/ngeo2355

deMenocal P, Ortiz J, Guilderson T, Adkins J, Sarnthein M, Baker L, Yarusinsky M. 2000. Abrupt onset and termination of the African Humid Period: Quaternary Science Reviews 19 : 347–361. DOI: 10.1016/S0277-3791(99)00081-5

Deng K, Yang S, Guo Y. 2022. A global temperature control of silicate weathering intensity. Nature Communications 13 : 1781. DOI: 10.1038/s41467-022-29415-0

Dixon JL, Nicholas GE, Pierce KL, Lageson D. 2024. Morphology, timing, and drivers of post-glacial landslides in the northern Yellowstone region. Earth Surface Processes and Landforms 49 : 3873–3888. DOI: 10.1002/esp.5943

Eppes M, Keanini R. 2017. Mechanical weathering and rock erosion by climate-dependent subcritical cracking. Reviews of Geophysics **55** : 470–508. DOI: 10.1002/2017RG000557

Faris F, Fawu W. 2014. Investigation of the initiation mechanism of an earthquake- induced landslide during rainfall: a case study of the Tandikat landslide, West Sumatra, Indonesia. Geoenvironmental Disasters 1 : 4. DOI: 10.1186/s40677-014-0004-3

Garelick S et al. 2022. The dynamics of warming during the last deglaciation in high-elevation regions of Eastern Equatorial Africa. Quaternary Science Reviews 281 : 107416. DOI: 10.1016/j.quascirev.2022.107416

Gariano SL, Guzzetti F. 2016. Landslides in a changing climate. Earth-Science Reviews 162 : 227–252. DOI: 10.1016/j.earscirev.2016.08.011

Garwood NC, Janos DP, Brokaw N. 1979. Earthquake-Caused Landslides: A Major Disturbance to Tropical Forests. Science 205 : 997–999. DOI: 10.1126/science.205.4410.997

Gerber E, Scheidegger AE. 1969. Stress-induced weathering of rock masses. DOI: 10.5169/SEALS-163705 [online] Available from: https://www.e-periodica.ch/digbib/view?pid=egh-001:1969:62::964 (Accessed 30 June 2025)

Gosse JC, Phillips FM. 2001. Terrestrial in situ cosmogenic nuclides: theory and application. Quaternary Science Reviews 20 : 1475–1560. DOI: 10.1016/S0277-3791(00)00171-2

Grämiger LM, Moore JR, Gischig VS, Ivy-Ochs S, Loew S. 2017. Beyond debuttressing: Mechanics of paraglacial rock slope damage during repeat glacial cycles. Journal of Geophysical Research: Earth Surface **122** : 1004–1036. DOI: 10.1002/2016JF003967

Hartmann J, Moosdorf N, Lauerwald R, Hinderer M, West AJ. 2014. Global chemical weathering and associated P-release — The role of lithology, temperature and soil properties. Chemical Geology **363** : 145–163. DOI: 10.1016/j.chemgeo.2013.10.025

Hartmeyer I, Delleske R, Keuschnig M, Krautblatter M, Lang A, Schrott L, Otto J-C. 2020. Current glacier recession causes significant rockfall increase: the immediate paraglacial response of deglaciating cirque walls. Earth Surface Dynamics 8 : 729–751. DOI: 10.5194/esurf-8-729-2020

Hayes JL, Riebe CS, Holbrook WS, Flinchum BA, Hartsough PC. 2019. Porosity production in weathered rock: Where volumetric strain dominates over chemical mass loss. Science Advances **5** : eaao0834. DOI: 10.1126/sciadv.aao0834

Hilger P, Gosse JC, Hermanns RL. 2019. How significant is inheritance when dating rockslide boulders with terrestrial cosmogenic nuclide dating?—a case study of an historic event. Landslides 16 : 729–738. DOI: 10.1007/s10346-018-01132-0

Hilger P, Hermanns RL, Gosse JC, Jacobs B, Etzelmüller B, Krautblatter M. 2018. Multiple rock-slope failures from Mannen in Romsdal Valley, western Norway, revealed from Quaternary geological mapping and10 Be exposure dating. The Holocene 28 : 1841–1854. DOI: 10.1177/0959683618798165

Iverson RM. 2000. Landslide triggering by rain infiltration. Water Resources Research 36 : 1897–1910. DOI: 10.1029/2000WR900090

Ivy-Ochs S, Poschinger A v., Synal H-A, Maisch M. 2009. Surface exposure dating of the Flims landslide, Graubünden, Switzerland. Geomorphology 103 : 104–112. DOI: 10.1016/j.geomorph.2007.10.024

Ivy-Ochs S, Schaller M. 2009. Chapter 6 Examining Processes and Rates of Landscape Change with Cosmogenic Radionuclides. In Radioactivity in the Environment , . Elsevier; 231–294. [online] Available from: https://linkinghub.elsevier.com/retrieve/pii/S1569486009016064 (Accessed 19 June 2025)

Jackson MS, Kelly MA, Russell JM, Doughty AM, Howley JA, Chipman JW, Cavagnaro D, Nakileza B, Zimmerman SRH. 2019. High-latitude warming initiated the onset of the last deglaciation in the tropics. Science Advances 5 : eaaw2610. DOI: 10.1126/sciadv.aaw2610

Jackson MS, Kelly MA, Russell JM, Doughty AM, Howley JA, Chipman JW, Cavagnaro DA, Baber MB, Zimmerman SRH, Nakileza B. 2020. Glacial fluctuations in tropical Africa during the last glacial termination and implications for tropical climate following the Last Glacial Maximum. Quaternary Science Reviews 243 : 106455. DOI: 10.1016/j.quascirev.2020.106455

Jacobs L, Dewitte O, Poesen J, Delvaux D, Thiery W, Kervyn M. 2016a. The Rwenzori Mountains, a landslide-prone region? Landslides 13 : 519–536. DOI: 10.1007/s10346-015-0582-5

Jacobs L, Dewitte O, Poesen J, Maes J, Mertens K, Sekajugo J, Kervyn M. 2017. Landslide characteristics and spatial distribution in the Rwenzori Mountains, Uganda. Journal of African Earth Sciences 134 : 917–930. DOI: 10.1016/j.jafrearsci.2016.05.013

Jacobs L, Maes J, Mertens K, Sekajugo J, Thiery W, Van Lipzig N, Poesen J, Kervyn M, Dewitte O. 2016b. Reconstruction of a flash flood event through a multi-hazard approach: focus on the Rwenzori Mountains, Uganda. Natural Hazards 84 : 851–876. DOI: 10.1007/s11069-016-2458-y

Jacquemart M et al. 2024. Detecting the impact of climate change on alpine mass movements in observational records from the European Alps. Earth-Science Reviews **258** : 104886. DOI: 10.1016/j.earscirev.2024.104886

Jess S, Koehn D, Fox M, Enkelmann E, Sachau T, Aanyu K. 2020. Paleogene initiation of the Western Branch of the East African Rift: The uplift history of the Rwenzori Mountains, Western Uganda. Earth and Planetary Science Letters 552 : 116593. DOI: 10.1016/j.epsl.2020.116593

Kaser, G., Osmaston, H., 2002. *Tropical glaciers*. Cambridge University Press.

Kelly MA, Russell JM, Baber MB, Howley JA, Loomis SE, Zimmerman S, Nakileza B, Lukaye J. 2014. Expanded glaciers during a dry and cold Last

Glacial Maximum in equatorial East Africa. Geology 42 : 519–522. DOI: 10.1130/G35421.1

Koehn D, Lindenfeld M, Rümpker G, Aanyu K, Haines S, Passchier CW, Sachau T. 2010. Active transsection faults in rift transfer zones: evidence for complex stress fields and implications for crustal fragmentation processes in the western branch of the East African Rift. International Journal of Earth Sciences 99 : 1633–1642. DOI: 10.1007/s00531-010-0525-2

Koehn D, Link K, Sachau T, Passchier CW, Aanyu K, Spikings A, Harbinson R. 2016. The Rwenzori Mountains, a Palaeoproterozoic crustal shear belt crossing the Albertine rift system. International Journal of Earth Sciences 105 : 1693–1705. DOI: 10.1007/s00531-015-1167-1

Krautblatter M, Funk D, Günzel FK. 2013. Why permafrost rocks become unstable: a rock–ice-mechanical model in time and space. Earth Surface Processes and Landforms 38 : 876–887. DOI: 10.1002/esp.3374

Lang A, Moya J, Corominas J, Schrott L, Dikau R. 1999. Classic and new dating methods for assessing the temporal occurrence of mass movements. Geomorphology 30 : 33–52. DOI: 10.1016/S0169-555X(99)00043-4

Lachner J, Rugel G, Vivo Vilches C, Koll D, Stübner K, Winkler S, Wallner A. 2023. Optimization of 10Be measurements at the 6 MV AMS facility DREAMS. Nuclear Instruments and Methods in Physics Research Section B: Beam Interactions with Materials and Atoms **535** : 29–33. DOI: 10.1016/j.nimb.2022.11.008

Larsen MC, Simon A. 1993. A Rainfall Intensity-Duration Threshold for Landslides in a Humid-Tropical Environment, Puerto Rico. Geografiska Annaler: Series A, Physical Geography 75 : 13–23. DOI: 10.1080/04353676.1993.11880379

Lifton N, Sato T, Dunai TJ. 2014. Scaling in situ cosmogenic nuclide production rates using analytical approximations to atmospheric cosmic-ray fluxes. Earth and Planetary Science Letters 386 : 149–160. DOI: 10.1016/j.epsl.2013.10.052

Lindenfeld M, Rümpker G, Batte A, Schumann A. 2012. Seismicity from February 2006 to September 2007 at the Rwenzori Mountains, East African Rift: earthquake distribution, magnitudes and source mechanisms. Solid Earth 3 : 251–264. DOI: 10.5194/se-3-251-2012

Livingstone DA. 1967. Postglacial Vegetation of the Ruwenzori Mountains in Equatorial Africa. Ecological Monographs 37 : 25–52. DOI: 10.2307/1948481

Maasha N. 1975. The seismicity of the Ruwenzori Region in Uganda. Journal of Geophysical Research 80 : 1485–1496. DOI: 10.1029/JB080i011p01485

Marc O, Hovius N, Meunier P, Uchida T, Hayashi S. 2015. Transient changes of landslide rates after earthquakes. Geology 43 : 883–886. DOI: 10.1130/G36961.1

Margirier A, Audin L, Carcaillet J, Schwartz S, Benavente C. 2015. Tectonic and climatic controls on the Chuquibamba landslide (western Andes, southern Peru). Earth Surface Dynamics 3 : 281–289. DOI: 10.5194/esurf-3-281-2015

Mason A, Russell J, Garelick S, Ivory S, Kelly M, Nakileza B, Anderson N. 2024. Hydroclimatic change and vegetation response in Tropical African alpine environments over the Holocene. Quaternary Science Reviews 344 : 108947. DOI: 10.1016/j.quascirev.2024.108947

McColl ST. 2012. Paraglacial rock-slope stability. Geomorphology 153–154 : 1–16. DOI: 10.1016/j.geomorph.2012.02.015

McColl ST, Davies TRH. 2013. Large ice-contact slope movements: glacial buttressing, deformation and erosion. Earth Surface Processes and Landforms 38 : 1102–1115. DOI: 10.1002/esp.3346

Merchel S, Herpers U. 1999. An Update on Radiochemical Separation Techniques for the Determination of Long-Lived Radionuclides via Accelerator Mass Spectrometry. ract 84 : 215–220. DOI: 10.1524/ract.1999.84.4.215

Osmaston H. 1989. Glaciers, glaciations and equilibrium line altitudes on the Ruwenzori. In Quaternary and environmental research on East African mountains , Mahaney WH (ed). CRC Press: Boca Raton;

Pánek T. 2015. Recent progress in landslide dating: A global overview. Progress in Physical Geography: Earth and Environment 39 : 168–198. DOI: 10.1177/0309133314550671

Pánek T. 2019. Landslides and Quaternary climate changes—The state of the art. Earth-Science Reviews 196 : 102871. DOI: 10.1016/j.earscirev.2019.05.015

Patton AI, Rathburn SL, Capps DM. 2019. Landslide response to climate change in permafrost regions. Geomorphology 340 : 116–128. DOI: 10.1016/j.geomorph.2019.04.029

Pei Y, Qiu H, Yang D, Liu Z, Ma S, Li J, Cao M, Wufuer W. 2023. Increasing landslide activity in the Taxkorgan River Basin (eastern Pamirs Plateau, China) driven by climate change. CATENA **223** : 106911. DOI: 10.1016/j.catena.2023.106911

Regmi D, Watanabe T. 2009. Rockfall activity in the Kangchenjunga area, Nepal Himalaya. Permafrost and Periglacial Processes **20** : 390–398. DOI: 10.1002/ppp.664

RGI 7.0 Consortium, 2023. Randolph Glacier Inventory - A Dataset of Global Glacier Outlines, Version 7.0. Boulder, Colorado USA. NSIDC: National Snow and Ice Data Center. doi:10.5067/f6jmovy5navz. Online access: https://doi.org/10.5067/f6jmovy5navz

Ring U. 2008. Extreme uplift of the Rwenzori Mountains in the East African Rift, Uganda: Structural framework and possible role of glaciations:

EXTREME UPLIFT OF RWENZORI MOUNTAINS. Tectonics 27 : n/a-n/a. DOI: 10.1029/2007TC002176

Roller S, Wittmann H, Kastowski M, Hinderer M. 2012. Erosion of the Rwenzori Mountains, East African Rift, from in situ-produced cosmogenic 10 Be: EROSION IN A TROPICAL MOUNTAIN RANGE. Journal of Geophysical Research: Earth Surface 117 : n/a-n/a. DOI: 10.1029/2011JF002117

Russell J, Eggermont H, Taylor R, Verschuren D. 2009. Paleolimnological records of recent glacier recession in the Rwenzori Mountains, Uganda-D. R. Congo. Journal of Paleolimnology 41 : 253–271. DOI: 10.1007/s10933-008-9224-4

Sewell RJ, Barrows TT, Campbell SDG, Fifield LK. 2006. Exposure dating (10Be,26Al) of natural terrain landslides in Hong Kong, China. In In Situ-Produced Cosmogenic Nuclides and Quantification of Geological Processes , . Geological Society of America; [online] Available from: https://pubs.geoscienceworld.org/books/book/570/chapter/3803210 (Accessed 11 December 2024)

Shanahan TM, McKay NP, Hughen KA, Overpeck JT, Otto-Bliesner B, Heil CW, King J, Scholz CA, Peck J. 2015. The time-transgressive termination of the African Humid Period. Nature Geoscience 8 : 140–144. DOI: 10.1038/ngeo2329

Stoffel M, Trappmann DG, Coullie MI, Ballesteros Cánovas JA, Corona C. 2024. Rockfall from an increasingly unstable mountain slope driven by climate warming. Nature Geoscience **17** : 249–254. DOI: 10.1038/s41561-024-01390-9

Tierney JE, Pausata FSR, deMenocal PB. 2017. Rainfall regimes of the Green Sahara. Science Advances 3 : e1601503. DOI: 10.1126/sciadv.1601503

Trauth MH, Bookhagen B, Marwan N, Strecker MR. 2003. Multiple landslide clusters record Quaternary climate changes in the northwestern Argentine Andes. Palaeogeography, Palaeoclimatology, Palaeoecology 194 : 109–121. DOI: 10.1016/S0031-0182(03)00273-6

Voigtländer A, Leith K, Krautblatter M. 2018. Subcritical Crack Growth and Progressive Failure in Carrara Marble Under Wet and Dry Conditions. Journal of Geophysical Research: Solid Earth **123** : 3780–3798. DOI: 10.1029/2017JB014956

Voigtländer A, Rheinwalt A, Tofelde S. 2024a. Quantifying Earth's Topography: Steeper and Larger Than Projected in Digital Terrain Models. Geophysical Research Letters **51** : e2024GL109517. DOI: 10.1029/2024GL109517

Voigtländer A et al. 2024b. Soft matter physics of the ground beneath our feet. Soft Matter **20** : 5859–5888. DOI: 10.1039/D4SM00391H

Walter B, Géraud Y, Bartier D, Kluska J-M, Diraison M, Morlot C, Raisson F. 2018. Petrophysical and mineralogical evolution of weathered crystalline basement in western Uganda: Implications for fluid transfer and storage. AAPG Bulletin 102 : 1035–1065. DOI: 10.1306/0810171610917171

White AF, Blum AE. n.d. Effects of climate on chemical, weathering in watersheds :

Wild B, Gerrits R, Bonneville S. 2022. The contribution of living organisms to rock weathering in the critical zone. npj Materials Degradation **6** : 98. DOI: 10.1038/s41529-022-00312-7

Worthington SRH, Davies GJ, Alexander EC. 2016. Enhancement of bedrock permeability by weathering. Earth-Science Reviews 160 : 188–202. DOI: 10.1016/j.earscirev.2016.07.002

Zerathe S, Audin L, Robert X, Schwartz S, Carcaillet J. 2022. Large landslide of the hyperarid Central Western Andes triggered during a humid period of the late Pleistocene (ca. 19°S; northern Chile). Terra Nova : ter.12641. DOI: 10.1111/ter.12641

Zerathe S, Lebourg T, Braucher R, Bourlès D. 2014. Mid-Holocene cluster of large-scale landslides revealed in the Southwestern Alps by 36Cl dating. Insight on an Alpine-scale landslide activity. Quaternary Science Reviews 90 : 106–127. DOI: 10.1016/j.quascirev.2014.02.015

Zhuang Y, Xing A, Jiang Y, Sun Q, Yan J, Zhang Y. 2022. Typhoon, rainfall and trees jointly cause landslides in coastal regions. Engineering Geology 298 : 106561. DOI: 10.1016/j.enggeo.2022.106561

Zogning A, Ngouanet C, Tiafack O. 2007. The catastrophic geomorphological processes in humid tropical Africa: A case study of the recent landslide disasters in Cameroon. Sedimentary Geology 199 : 13–27. DOI: 10.1016/j.sedgeo.2006.03.030